Spacer-Based Selectivity in the Binding of "Two-Prong" Ligands to Recombinant Human Carbonic Anhydrase I†

Abir L. Banerjee, Daniel Eiler, Bidhan C. Roy, Xiao Jia, Manas K. Haldar, Sanku Mallik,* and D. K. Srivastava*

Department of Chemistry, Biochemistry and Molecular Biology, North Dakota State University, Fargo, North Dakota 58105

Received October 22, 2004; Revised Manuscript Received December 18, 2004

ABSTRACT: Benzenesulfonamide and iminodiacetate (IDA)-conjugated Cu^{2+} independently interact at the active site and a peripheral site of carbonic anhydrases, respectively [Banerjee, A. L., Swanson, M., Roy, B. C., Jia, X., Haldar, M. K., Mallik, S., and Srivastava, D. K. (2004) *J. Am. Chem. Soc. 126*, 10875−10883]. By attaching IDA-bound Cu^{2+} to benzenesulfonamide via different chain length spacers, we synthesized two "two-prong" ligands, **L1** and **L2**, in which the distances between Cu^{2+} and NH_2 group of sulfonamide were 29 and 22 Å, respectively. We compared the binding affinities of **L1** and **L2**, vis-à-vis their parent compound, benzenesulfonamide, for recombinant human carbonic anhydrase I (hCA-I) by performing the fluorescence titration and steady-state kinetic experiments. The experimental data revealed that whereas the binding affinity of **L1** for hCA-I was similar to that of benzenesulfonamide, the binding affinity of **L2** was ∼2 orders of magnitude higher, making **L2** one of the most potent ligands or inhibitors of hCA-I. Since the enhanced binding or inhibitory potency of **L2** is diminished (to the level of benzenesulfonamide) either in the presence of EDTA or upon treatment of the enzyme with diethyl pyrocarbonate, it is proposed that Cu^{2+} of **L2** interacts with one of the surface-exposed histidine residues of the enzyme. A cumulative account of the experimental data leads to the suggestion that the differential binding of **L1** versus **L2** to hCA-I is encoded in the chain length of the spacer moiety.

Carbonic anhydrases (CAs,[1] EC 4.2.1.1) are ubiquitously distributed zinc-containing metalloenzymes, which are involved in a variety of physiological functions (*1*, *2*). In the animal kingdom, there are 15 isozymes of carbonic anhydrases, of which five isozymes (CA-I, CA-II, CA-III, CA-VII, and CA-XIII) are cytosolic, two (CA-VA and CA-VB) are mitochondrial, one (CA-VI) is secreted, four (CA-IV, CA-IX, CA-XII, and CA-XIV) are membrane-associated (*3*), and the remaining three (CA-VIII, CA-X, and CA-XI) are also cytosolic but do not exhibit any catalytic activity (*4*). Recent evidence suggests that CA-VIII, CA-IX, and CA-XII are involved in tumorigenesis (*4*). The catalytic CAs promote reversible hydration of CO_2 in forming HCO_3^-, which is involved in a variety of biosynthetic reactions, such as gluconeogenesis, synthesis of certain amino acids (via pyruvate carboxylase), lipogenesis (via acetyl-CoA carboxylase), ureagenesis (via carbamoyl phosphate synthetase I), and pyrimidine nucleotide biosynthesis (via carbamoyl phosphate synthetase II) (*2*). Besides, these enzymes are involved in pH homeostasis, ion transport, water and electrolyte balance, bone resorption, calcification, and tumorigenesis (*5*).

Carbonic anhydrases have been the targets of drug designing by major pharmaceutical companies since the 1950s, and a variety of highly potent inhibitors initially emerged as drugs for the treatments of different pathological conditions, such as glaucoma, hypertension, convulsion and epilepsy, altitude sickness, obesity, diabetes, etc. (*6*−*11*). However, because of serious side effects, several highly potent carbonic anhydrase inhibitors could not pass the scrutiny of trial phases (*1*, *12*). Currently, dorzolamide and brinzolamide are the only two carbonic anhydrase inhibitors which have been approved for topical applications for the treatment of chronic glaucoma (*12*). One of the main reasons for the side effects of carbonic anhydrase inhibitors (mostly the sulfonamide derivatives) has been their indiscriminate inhibitory effects on different isozymes (*1*, *2*). This is not surprising because of the marked similarity in the active site pockets of carbonic anhydrase isozymes (*13*).

We recently became interested in designing the isozyme specific inhibitors of carbonic anhydrases (*14*, *15*). Using the recombinant form of human carbonic anhydrase II (hCA-II), we demonstrated that the binding affinity of its active site-directed inhibitor, benzenesulfonamide, is enhanced by ∼40-fold by attaching it with iminodiacetic acid (IDA)-conjugated Cu^{2+} via a spacer ("two-prong" inhibitor) (*16*). On the basis of the literature precedents as well as the molecular modeling data, we proposed that whereas the benzenesulfonamide group of the inhibitor binds to the active site of hCA-II, the IDA−Cu^{2+} group loops around and binds to one of the surface-exposed histidine (His-4) residues of the enzyme (*15*). Although this has been our working hypothesis, we did not have compelling data to justify the

† This research was supported by National Institutes of Health Grants 1R15 DK56681-01A1 to D.K.S. and 1R01 GM 63404-01A1 to S.M.

* To whom correspondence should be addressed. D.K.S.: telephone, (701) 231-7831; fax, (701) 231-7884; e-mail, dk.srivastava@ndsu.nodak.edu. S.M.: telephone, (701) 231-8829; fax, (701) 231-8831; e-mail, sanku.mallik@ndsu.nodak.edu.

[1] Abbreviations: IDA, iminodiacetic acid; CA, carbonic anhydrase; **L1**, ligand 1; **L2**, ligand 2; hCA-I, human carbonic anhydrase I; hCA-II, human carbonic anhydrase II; EDTA, ethylenediaminetetraacetic acid; DEPC, diethyl pyrocarbonate; DMF, dimethylformamide; CDMT, chlorodimethoxytriazine.

10.1021/bi047737b CCC: $30.25
Published on Web 02/10/2005

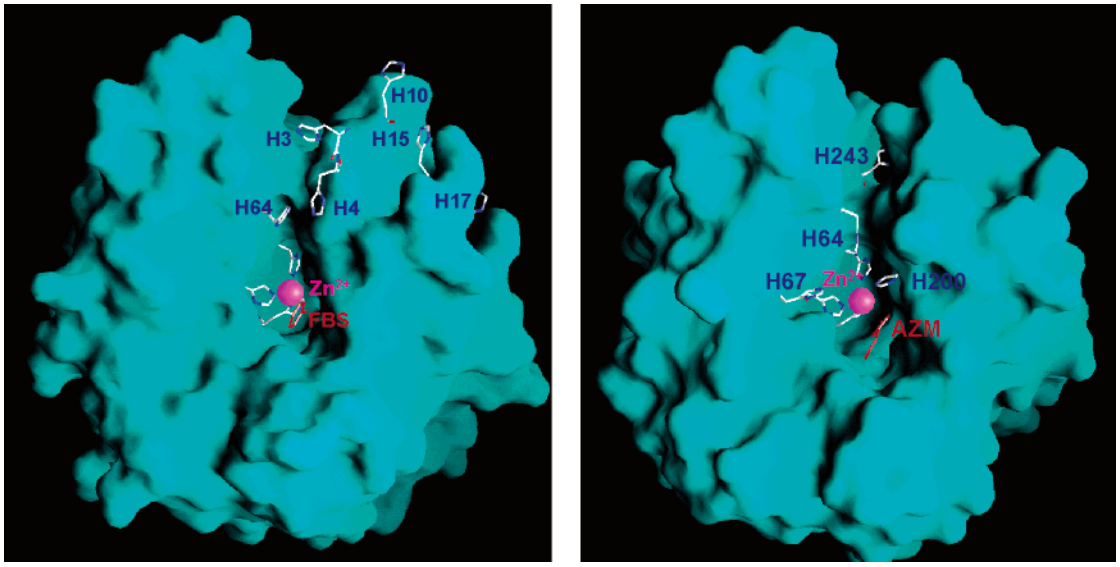

FIGURE 1: Molecular surfaces of human carbonic anhydrase I (left) and human carbonic anhydrase II (right) structures, showing the surface-exposed histidine residues, Zn^{2+}, and the bound sulfonamide derivatives. The surface maps have been created with the aid GRASP (17) on the SGI molecular modeling workstation. The histidine residues involved in coordinating Zn^{2+} are not labeled. In this view, whereas His-64, His-67, His-200, and His-243 represent the surface-exposed histidine residues in the case of hCA-I, His-64, His-4, His-3, His-10, His-15, and His-17 represent the surface-exposed histidine residues in the case of hCA-II. The sulfonamide derivatives in hCA-I and hCA-II are 5-acetamido-1,3,4-thiadiazole-2-sulfonamide (AZM) and 4-fluorobenzenesulfonamide (FBS), respectively.

interaction of the IDA−Cu^{2+} group of two-prong ligands with histidine. The experimental results presented herein corroborate the notion that the IDA−Cu^{2+}-assisted enhancement in the binding affinity of the ligands indeed comes from the interaction of Cu^{2+} with "one" surface-exposed histidine residue(s) of hCA-I.

A casual perusal of the X-ray crystallographic structures of different carbonic anhydrase isozymes reveals that although their active sites are remarkably similar, the spatial distribution of the surface-exposed histidine residues is quite different (*13*). This is not surprising since the surface-exposed residues of independently functioning proteins are unlikely to be conserved during the course of evolution (*17*). When the structures of hCA-I and hCA-II are compared, it is evident that the spatial distribution of the surface-exposed histidine residues is considerably different. As shown in Figure 1, there are six closely spaced histidine residues (namely, His-3, His-4, His-10, His-15, His-17, and His-64) near the N-terminal end of hCA-II. In contrast, in the case of hCA-I, except for His-64, none of the above-noted N-terminal residues are conserved. Although His-64 is common to hCA-I and hCA-II, its functional role as a proton "translocator" is justifiable only in the case of the latter enzyme (*18*, *19*). In the case of hCA-I, three new histidine residues (namely, His-67, His-200, and His-243), which are not so closely spaced, predominate near the active site cavity of the enzyme (*13*, *20*, *29*). This feature of hCA-I attracted our attention for investigating the spacer-based selectivity of two-prong ligands. Given the limited number of surface-exposed histidine residues, as well as their localization in the vicinity of the active site pocket, we became interested in investigating whether the high-affinity ligands can be rationally designed by controlling the distance between the benzenesulfonamide and IDA−Cu^{2+} groups of two-prong ligands. As will be shown in the next section, we synthesized two two-prong ligands, which differed with respect to the spacer chain length by 7 Å. Of these ligands, only the shorter spacer-containing ligand could interact with the enzyme via both prongs, emerging as one of the most potent inhibitors of hCA-I. The longer spacer-containing ligand, on the other hand, exhibited a binding affinity similar to that of its parent ligand, benzenesulfonamide, suggesting that it only interacted with the enzyme via its active site-directed prong, benzenesulfonamide, and the other (IDA−Cu^{2+}) prong remained unused.

EXPERIMENTAL PROCEDURES

Materials

Zinc sulfate, ampicillin, chloramphenicol, and IPTG were purchased from Life Science Resources (Milwaukee, WI). Yeast extracts and tryptone were purchased from Becton Dickinson (Sparks, MD). Acetonitrile was from Aldrich Chemicals (Milwaukee, WI). HEPES, *p*-aminomethylbenzenesulfonamide agarose, *p*-nitrophenyl acetate, and PMSF were obtained from Sigma. Dansylamide was purchased from Avocado Research Chemicals (Heysham, Lancashire, U.K.). All the chemicals needed for synthesis of **L1** and **L2** were purchased from Aldrich Chemicals. The BL21codon plus DE3(RIL) expression cells were from Stratagene (La Jolla, CA). All other chemicals were reagent grade, and were used without further purification.

The plasmid containing the coding sequence of hCA-I (pCMV-SPORT6) was obtained from Open Biosystems (Huntsville, AL).

Methods

*Synthesis of Ligands. (1) Compound **2***. To a solution of the acid **1** (*28*) (1.00 g, 4.04 mmol) in ethyl acetate (30 mL) was added *N*-hydroxysuccinimide (0.5 g, 0.435 mmol) followed by the addition of DCC (0.90 g, 4.36 mmol). The resulting solution was stirred at room temperature for 45 min. The white solid was filtered and washed with ethyl acetate, and the solvent from the filtrate was removed under reduced pressure. The viscous liquid was again dissolved in $CHCl_3$

(30 mL). The *p*-aminobenzoic acid was dissolved in $CHCl_3$ (10 mL) in the presence of Et_3N (0.8 mL, 5.75 mmol) and added to the solution described above. The reaction was continued for an additional 8 h at room temperature. The organic layer was washed with water and dried with anhydrous Na_2SO_4. The crude product was purified by silica gel column chromatography with 15% MeOH in $CHCl_3$ to give pure **2** as a viscous liquid (R_f = 0.3): 0.97 g yield (64%); ^{1}H NMR (400 MHz, $CDCl_3$) δ 1.27−1.33 (m, 6H), 3.58 (s, 2H), 3.65 (s, 4H), 4.19−4.26 (m, 4H), 7.83 (d, 2H, J = 8.5 Hz), 7.93 (bs, 1H), 8.11 (d, 2H, J = 8.5 Hz).

*(2) Ligand **L1***. To a solution of acid **2** (0.18 g, 0.49 mmol) in $CHCl_3$ (20 mL) was added compound **3** (*14*) (0.22 g, 0.598 mmol) followed by the addition of BOP reagent (0.22 g, 0.50 mmol) and Et_3N (0.25 mL, 1.8 mmol). The reaction mixture was stirred at the room temperature for 12 h. The workup procedure was the same as mentioned before for compound **2**. The crude product was purified by silica gel column chromatography with 8% MeOH in $CHCl_3$ (R_f = 0.2) to obtain the pure compound as a viscous liquid: 0.22 g yield (63%); ^{1}H NMR (500 MHz, $CDCl_3$/CD_3OD/D_2O) δ 1.25−1.29 (m, 6H), 3.40 (s, 2H), 3.54−3.71 (m, 16H), 4.16−4.22 (m, 4H), 7.71 (d, 2H, J = 8.2 Hz), 7.81 (d, 2H, J = 8.2 Hz), 7.87−7.92 (m, 4H); ^{13}C NMR (125 MHz, $CDCl_3$/CD_3OD) δ 25.01, 25.71, 30.13, 33.87, 36.74, 39.79, 39.99, 55.25, 56.45, 60.22, 60.91, 61.54, 70.24, 70.35, 119.12, 126.49, 127.89, 128.25, 129.57, 137.64, 140.89, 145.55, 167.66, 170.75, 171.12, 171.89.

The above ester (0.12 g, 0.16 mmol) was dissolved in MeOH (6 mL) and CH_2Cl_2 (3 mL), and solid LiOH (25 mg, 0.59 mmol) was added. The reaction mixture was stirred at room temperature for 12 h. The pH of the solution was lowered to 3 by adding concentrated HCl. The organic solvent was removed under vacuo, and the precipitated solid was filtered, washed with absolute EtOH and THF/MeOH (1:1) and then dried: 90 mg yield (81%); ^{1}H NMR (300 MHz, D_2O) δ 3.30 (s, 4H), 3.52−3.58 (m, 12H), 3.69 (s, 2H), 7.52−7.55 (m, 2H), 7.67 (m, 4H), 7.78−7.84 (m, 2H).

The above acid (80 mg, 0.121 mmol) was dissolved in MeOH (8 mL), and solid $CuCl_2 \cdot 2H_2O$ (21 mg, 0.123 mmol) was added. The mixture was stirred at room temperature for 6 h. The solvent was removed under vacuum, and the semisolid thus obtained was dissolved in a minimal volume of absolute EtOH (1 mL) and THF (4 mL). It was precipitated by the addition of CH_2Cl_2 (6 mL) to this solution. The solid was filtered, washed with ether, and dried under vacuum: 55 mg yield (61%). Anal. Calcd for $C_{26}H_{31}CuN_5O_{11}S \cdot H_2O$: C, 44.41; H, 4.51; N, 9.96. Found: C, 44.65; H, 4.51; N, 10.07.

*(3) Compound **6***. To a stirred solution of Boc-Lys(Cbz)-OH (2 g, 5.26 mmol) in $CHCl_3$ (40 mL) and DMF (10 mL) were added chlorodimethoxytriazine (CDMT, 1.1 g, 6.27 mmol) and *N*-methylmorpholine (1.4 mL, 12.75 mmol). The solution was stirred at room temperature for 15 min followed by the dropwise addition of a solution of *p*-(2-aminoethyl)-benzenesulfonamide (1.059 g, 5.26 mmol) in DMF (5 mL). Stirring was continued at room temperature for 12 h. The reaction was quenched with brine, and the solvents were removed under reduced pressure. Water was added to the residue and extracted with ethyl acetate. Purification of the crude product by silica gel column chromatography (eluting first with chloroform and then with 4% MeOH in chloroform) afforded the pure product as a viscous liquid (R_f = 0.3, 4% MeOH/$CHCl_3$; 2.3 g, 78%): ^{1}H NMR (300 MHz, $CDCl_3$) δ 1.16−1.27 (m, 2H), 1.36 (s, 9H), 1.39−1.55 (m, 2H), 1.60−1.71 (m, 2H), 2.77−2.86 (m, 2H), 3.02−3.11 (m, 2H), 3.36−3.56 (m, 2H), 3.92−4.01 (m, 1H), 5.03 (s, 2H), 6.61 (br s, 1H), 7.23−7.30 (m, 7H), 7.76 (d, 2H, J = 8.4 Hz).

The above product (1.22 g, 2.17 mmol) was treated with 10 mL of 4 N HCl in dioxane for 6 h at room temperature. Removal of the solvent and drying under high vacuum for 4 h yielded the deprotected amine (as the HCL salt, 1.0 g, 92%). The product was sufficiently pure and was used in the next step: ^{1}H NMR (300 MHz, $CDCl_3$) δ 1.14−1.19 (m, 2H), 1.35−1.39 (m, 2H), 1.61−1.66 (m, 2H), 2.82−2.85 (m, 2H), 2.96−3.04 (m, 2H), 3.47−3.6 (m, 2H), 3.79 (br s, 1H), 5.00 (s, 2H), 7.27−7.30 (m, 7H), 7.76 (d, 2H, J = 6.9 Hz).

To a stirred solution of this amine salt (2.9 g, 5.81 mmol) in $CHCl_3$ (50 mL) and DMF (15 mL) were added CDMT (1.13 g, 6.43 mmol) and *N*-methylmorpholine (3 mL, 27 mmol). The solution was stirred at room temperature for 15 min. Acid **1** (1.44 g, 5.82 mmol) in 5 mL of DMF was added to the reaction mixture slowly and the mixture stirred for 15 h at room temperature. The workup procedure was the same as described previously for the CDMT reaction. Purification was performed by silica gel column chromatography (eluting first with chloroform and then with 5% MeOH in chloroform, R_f = 0.3 in 5% MeOH/chloroform), yielding pure **6** as a colorless viscous liquid (3.1 g, 76%): ^{1}H NMR (300 MHz, $CDCl_3$) δ 1.22−1.29 (m, 6H), 1.45−1.51 (m, 2H), 1.59−1.68 (m, 2H), 1.76−1.85 (m, 2H), 2.81−2.89 (m, 6H), 3.11−3.25 (m, 2H), 3.42−3.55 (m, 4H), 4.1−4.18 (m, 4H), 4.28−4.38 (m, 1H), 5.064 (s, 2H), 7.26−7.34 (m, 7H), 7.78−7.83 (m, 2H).

*(4) Ligand **L2***. Compound **6** (700 mg, 1.01 mmol) was taken in 5% MeOH in water (10 mL), and a pinch of Pd black was added to it. The reaction mixture was refluxed for 8 h with continuous bubbling of hydrogen gas. Filtration of the catalyst and evaporation of solvent followed by drying under high vacuum yielded the product as a viscous liquid (524 mg, 93%): ^{1}H NMR (400 MHz, $CDCl_3$) δ 1.21−1.27 (m, 6H), 1.45−1.48 (m, 2H), 1.53−1.62 (m, 2H), 1.75−1.84 (m, 1H), 2.77−2.90 (m, 2H), 3.10−3.17 (m, 1H), 3.44−3.69 (m, 10H), 4.10−4.16 (m, 4H), 4.24−4.33 (m, 1H), 6.88 (br s, 1H), 7.27 (d, 2H, J = 8 Hz), 7.49 (br s, 1H), 7.79 (d, 2H, J = 8 Hz), 8.18 (br s, 1H).

This compound (150 mg, 0.27 mmol) was dissolved in a MeOH/CH_2Cl_2 mixture (10 mL) and treated with LiOH (35 mg, 1.45 mmol) for 12 h at room temperature. The solvents were evaporated under reduced pressure, and the residue was dissolved in water (10 mL). The pH of the solution was adjusted to 3 with careful addition of HCl (2 N). Water was removed under reduced pressure, and the residue was dried under vacuum. Addition of absolute ethanol to this viscous liquid led to the precipitation of a white solid. The solid thus obtained was filtered, washed with absolute ethanol, and dried under vacuum (110 mg, 81%): ^{1}H NMR (400 MHz, D_2O) δ 1.11−1.25 (m, 2H), 1.50−1.63 (m, 2H), 1.67−1.78 (m, 2H), 2.70−2.86 (m, 2H), 3.22−3.41 (m, 2H), 3.59−3.75 (m, 2H), 3.82−3.96 (m, 5H), 4.49 (s, 2H), 7.34 (d, 2H, J = 8.1 Hz), 7.73 (s, 1H), 7.78 (d, 2H, J = 8.1 Hz), 7.93 (s, 1H).

The sulfonamide diacid (63.5 mg, 0.127 mmol) was dissolved in 7 mL of a MeOH/H_2O mixture (6:1). Solid $CuCl_2 \cdot 2H_2O$ (22 mg, 0.129 mmol) was added to it, and the reaction mixture was stirred for 3 h at room temperature. The solvent was removed under reduced pressure, and trituration with absolute ethanol afforded a blue solid. This solid was filtered, washed with plenty of ethanol, and dried under vacuum to afford ligand **L2** (67 mg, 91%). Anal. Calcd for $C_{20}H_{29}CuN_5O_8S \cdot H_2O$: C, 41.34; H, 5.38; N, 12.05. Found: C, 41.47; H, 5.68; N, 11.88.

Cloning, Expression, and Purification of the Recombinant Human Carbonic Anhydrase I (hCA-I). The coding sequence of hCA-I (pCMV-SPORT6 plasmid) was amplified by the hot start PCR method (*21*), using the sense and antisense primers (5′-GGAATTCCATATGGCAAGTCCAGACTGGG-3′ and 5′-CCGCTCGAGTTAAAATGAAGCTCTCACT-GTTC-3′, respectively). These primers contained the *Nde*I and *Xho*I (underlined) restriction cleavage sites. The PCR mixture contained the template DNA (~0.1 μg), primers (2 μM), dNTPs (1 mM), $MgCl_2$ (5 mM), and *Pfu* DNA polymerase (0.05 unit) in a total volume of 50 μL. The PCR conditions were as follows: 1 min at 95 °C for denaturation, 1 min at 55 °C for annealing, and 2 min at 72 °C for extension, for a total number of 30 reaction cycles. The final products were allowed to extend for an additional 20 min. The PCR product and the expression vector pET-20b(+) were digested with *Nde*I and *Xho*I and purified via the Qiaquick gel extraction kit. The purified products were ligated by T4 DNA ligase and transformed into DH5α cells for plasmid propagation (*21*). The positive clones of hCA-I were confirmed by sequencing the plasmid at University of Chicago Cancer Research Center (Chicago, IL). The plasmid vector containing the hCA-I sequence was named pET-hCA-I.

Expression and Purification of Recombinant Human Carbonic Anhydrase I (hCA-I). The cloned plasmid (pET-hCA-I) was transformed into *Escherichia coli* BL21codon plus DE3(RIL) host cells by following the standard molecular biology protocol (*21*). The overnight culture of the expression cells from a freshly transformed plate was used to inoculate in 1 L of LB medium containing 100 μg/mL ampicillin, 50 μg/mL chloramphenicol, and 60 μM $ZnSO_4$ at 37 °C, with constant agitation at 250 rpm in an Environ orbital shaker, until the absorbance was 0.6 at 600 nm. The culture was induced by 400 μM IPTG and 400 μM $ZnSO_4$, and incubated overnight at 25 °C with constant shaking. The cells were harvested by centrifugation at 5000*g* for 15 min; pellets were washed in 50 mM Na_2HPO_4 and 0.15 M NaCl (pH 7.2) and resuspended in the same buffer, containing 1 mM phenylmethanesulfonyl fluoride (PMSF, prepared in 2-propanol). The cell suspension was sonicated by a Branson sonifier, using a 40% duty cycle in an ice cold bath (with intermittent cooling) for a total time of 5 min. The cell extracts thus obtained were centrifuged at 15 000 rpm for 30 min, and the supernatant (crude extract, total volume of 20 mL) was collected for purification of the enzymes by the following method.

The isozyme hCA-I was purified by the metal ion affinity chromatography using the IDA-conjugated Sepharose matrix. The matrix was prepared as described previously (*22*). For purification of hCA-I from the crude extract, the Sepharose−IDA column (2 cm × 12 cm) was charged with Cu^{2+} by passing approximately 1 bed volume of a 0.3 M $CuSO_4$ solution, followed by washing the column with 2 volumes of 0.5 M NaCl. The column was finally equilibrated by the cell lysis buffer [50 mM Na_2HPO_4 and 0.15 M NaCl (pH 7.2)]. The crude extract was applied to the column, and the column was thoroughly washed by the equilibration buffer containing 1 mM imidazole. Practically no hCA-I was found to elute off the column during the washing. The bound hCA-I was eluted by applying a gradient of 1 to 200 mM imidazole in the above buffer. The fractions containing the enzyme activity were pooled, concentrated, dialyzed against 25 mM HEPES buffer (pH 7.0), and stored at −20 °C.

The enzyme activity of the recombinant hCA-I was measured in 25 mM HEPES buffer (pH 7.0) containing 10% acetonitrile (the standard buffer) at 25 °C, using 0.4 mM *p*-nitrophenyl acetate as a substrate (*23*). The protein concentration was determined according to the Bradford method, utilizing BSA as the standard protein (*24*).

Spectrofluorometric Studies. All spectrofluorometric studies involving dansylamide were performed on a Perkin-Elmer lambda 50-B spectrofluorometer, equipped with a magnetic stirrer and thermostated water bath. To ensure the stability of dansylamide during the course of the titration as well as kinetic experiments, its stock solution (1 mM) was prepared in 10 mM HCl, and was diluted in the standard HEPES buffer containing 10% acetonitrile. The emission spectra of dansylamide in the absence and presence of hCA-I and hCA-II were acquired by fixing the excitation wavelength at 330 nm (excitation and emission slits each equal to 5 mm) with a cutoff filter at 390 nm.

The dissociation constant of the hCA-I−dansylamide complex was determined by titrating a fixed concentration of the enzyme (1 μM) with increasing concentrations of dansylamide in 25 mM HEPES buffer (pH 7.0) containing 10% acetonitrile. The initial reaction volume was 2.0 mL. The excitation and emission wavelengths were maintained at 330 and 448 nm, respectively, with a cutoff filter at 390 nm. The dissociation constant of the enzyme−dansylamide complex was determined by analyzing the binding isotherm as described by Qin and Srivastava (*25*).

The dissociation constant of the hCA-I−inhibitor complex was determined by competitive displacement of a fixed concentration of dansylamide by increasing concentrations of the inhibitor. In a typical experiment, an equilibration mixture containing 1 μM hCA-I and 10 μM dansylamide in the standard HEPES buffer (pH 7.0, containing 10% acetonitrile) was titrated with increasing concentrations of the inhibitor. The initial reaction volume was 2.0 mL, and the reaction content was continuously stirred during the course of the titration. The excitation and emission wavelengths were maintained at 330 and 448 nm, respectively, with a cutoff filter at 390 nm. Since the binding of the inhibitor competitively displaced dansylamide from the enzyme site, the fluorescence intensity at 448 nm decreased. The data were analyzed by a modified form of the competitive binding model as elaborated by Kumar and Srivastava (*26*).

$$[EB] = ([E]_t + [B]_t + K_b + (K_b/K_d)[D]_t) - \frac{([E]_t + [B]_t + K_b + (K_b/K_d)[D]_t)^2 - 4[E]_t[B]_t}{2} \quad (1)$$

The dissociation constant of the enzyme−inhibitor complex was determined by monitoring the decrease in the fluorescence of the enzyme−dansylamide complex (λ_{ex} = 330 nm, λ_{em} = 448 nm) as a function of the increasing concentration of the inhibitor. Hence, the observed fluorescence (F_{obs}) as a function of the inhibitor ([B]) concentration can be given by eq 2

$$F_{obs} = \Delta F_{max}/[E]_t \times ([E]_t - [EB]) \quad (2)$$

where ΔF_{max} is the maximum change in fluorescence upon complete displacement of dansylamide from the enzyme site. The titration data of Figure 4 were fitted by the nonlinear regression analysis of eq 2 using Grafit 4.

Steady-State Kinetics for the Inhibition of hCA-I. The steady-state kinetic experiments for the hCA-I-catalyzed reaction were performed on a Perkin-Elmer Lambda 3B spectrophotometer. All steady-state experiments were performed in the standard HEPES buffer, containing 10% acetonitrile. The latter solvent ensured the solubility of the substrate during the course of the reaction, and it did not exhibit any influence on the catalytic activity of the enzyme. The initial rates of the enzyme-catalyzed reactions were measured by following the hydrolysis of the chromogenic substrate, *p*-nitrophenyl acetate, at 348 nm (*23*).

The steady-state kinetic experiments were performed in a total reaction volume of 1.3 mL (in the standard buffer), containing 1 mM *p*-nitrophenylacetate and varied concentrations of the inhibitors. The initial rates of enzyme catalysis were determined by taking the slopes of the reaction traces. For easy comparison of the inhibition data, the initial rates were translated into percent activity as a function of the inhibitor concentrations.

Because of the slow esterase activity of hCA-I, a fairly high concentration of the enzyme (~2 μM) is utilized to reliably measure the initial rates of the enzyme reaction. With such a high concentration of the enzyme, part of the substrate and/or inhibitor can be envisaged to be bound to the enzyme site. Since the Michaelis−Menten equation relies on the free rather than the total concentrations of the substrates and inhibitors, the fraction of the bound species must be subtracted from their total concentrations for analyzing the kinetic data. Given the above constraints, the K_i values of the enzyme−ligand complexes were determined according to the best fit of the experimental data by eq 3, using the nonlinear regression analysis software, Grafit 4.0.

$$v = \frac{v_0 K_i}{K_i + \{[I]_t - 0.5[([I]_t + [E]_t + K_i) - \sqrt{([I]_t + [E]_t + K_i)^2 - 4[I]_t[E]_t}]\}} \quad (3)$$

Transient Kinetic Experiments. Transient kinetic experiments were performed on an Applied Photophysics SX-18 MV stopped-flow system, equipped with both absorption- and fluorescence-detecting photomultiplier tubes. The dead time of the stopped flow was 1.3 ms. For fluorescence measurement, the light path was configured such that the fluorescence photomultiplier detected the emitting light via the 2 mm path length. The excitation wavelength was maintained at 330 nm, and a 335 nm cutoff filter was installed at the entrance of the photomultiplier tube. The stopped-flow traces were analyzed by the data analysis package provided by Applied Photophysics.

For measuring the dissociation "off rates" of two-prong ligands from the hCA-I−ligand complexes, the reaction mixture containing hCA-I and individual ligands, in the standard HEPES buffer, were mixed with 100 μM dansylamide via the stopped-flow syringes. The time course of the increase in the fluorescence intensity was monitored. The data were analyzed by the single-exponential rate equation.

Isothermal Titration Microcalorimetric Studies. All calorimetric experiments were performed on an MCS isothermal titration calorimeter (ITC). A complete description of its predecessor instrument, OMEGA-ITC, experimental strategies, and data analysis are given by Wiseman et al. (*27*). The calorimeter was calibrated by known heat pulses as described in the MCS-ITC manual. During titration, the reference cell was filled with a 0.03% azide solution in water. Prior to the titration experiment, both the enzyme and ligand solution were thoroughly degassed. The sample cell was filled either with 1.8 mL (effective volume of 1.36 mL) of buffer (for control) or with an appropriately diluted enzyme. The contents of the sample cell were titrated with several aliquots (4 μL each) of the ligand. During the titration, the reaction mixture was constantly stirred at 400 rpm. The enzyme concentration was adjusted by 2% (as recommended by the manufacturer) to include a dilution effect of the enzyme solution, which occurs following a buffer rinse.

All calorimetric titration data were presented after subtracting the background signal, deduced from the magnitude of heat pulses at the end of the titration. The raw experimental data were presented as the amount of heat produced per second following each injection of ligand into the enzyme solution (minus the blank) as a function of time. The amount of heat produced per injection was calculated by integration of the area under individual peaks by the Origin software. Final data are presented as the amount of heat produced per injection versus the molar ratio of ligand to enzyme. The data were analyzed according to the method of Wiseman et al. (*27*).

The data analysis produced three parameters, viz., the stoichiometry (n), the association constant (K_a), and the standard enthalpy changes ($\Delta H°$) for the binding of **L2** to hCA-I. The standard free energy change ($\Delta G°$) for the binding was calculated according to the relationship $\Delta G° = -RT \ln K_a$. Given the magnitudes of $\Delta G°$ and $\Delta H°$, the standard entropy changes ($\Delta S°$) for the binding process were calculated according to the standard thermodynamic equation $\Delta G° = \Delta H° - T\Delta S°$.

Modification of Histidine Residues of hCA-I by Diethyl Pyrocarbonate. The covalent modification of histidine residues of human carbonic anhydrase I was achieved by incubating the enzyme with diethyl pyrocarbonate (DEPC) in 0.1 M sodium phosphate buffer (pH 6.0). Freshly prepared DEPC (in absolute ethanol) was added to the enzyme solution in the buffer described above, and the time course of the increase in absorption at 242 nm was monitored. Once the A_{242} value reached its maximum, the modification of the histidine residues of the enzyme was taken to be complete. For performance of the binding studies, the DEPC-incubated enzyme was subjected to gel filtration on a G-25 Sephadex column [equilibrated with 25 mM HEPES buffer (pH 7.0)] and utilized for the assessment of the enzyme−ligand

Scheme 1: Synthesis of Ligand **L1**

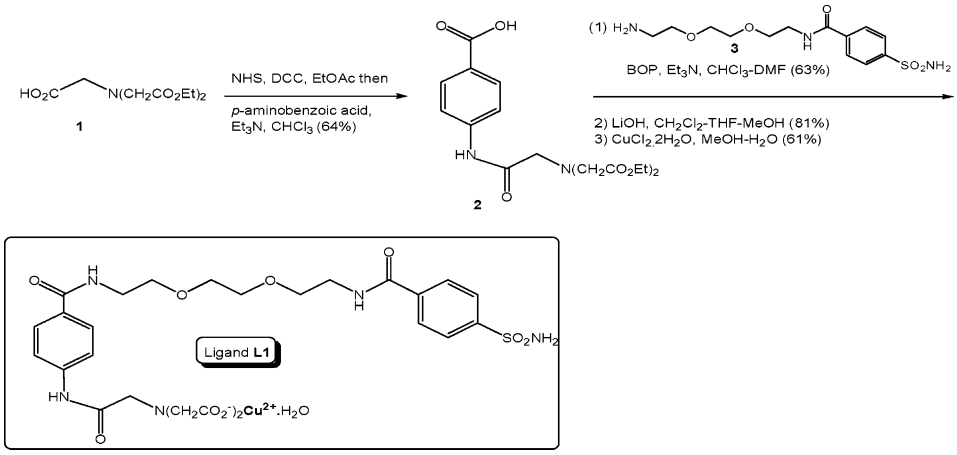

complexes. For determining the stoichiometry of modification of the enzyme's histidine residues, 10 μM hCA-I was titrated with increasing concentrations of DEPC in 0.1 M sodium phosphate buffer (pH 6.0), and the increases in absorption at 242 nm were recorded. The control experiment involved incubation of identical concentrations of DEPC in buffer. The difference in A_{242} between the sample and control experiments was plotted as a function of the ratio of DEPC to hCA-I to determine the stoichiometry of the enzyme's histidine modification by DEPC in the presence of saturating concentrations of benzenesulfonamide and **L2**.

Molecular Modeling Studies. The molecular modeling studies were performed on a Silicon Graphics-O2 molecular modeling workstation with the aid of Accelrys software, InsightII(98), Discover, and biopolymers. The coordinates for the X-ray crystallographic structure of human carbonic anhydrase I complexed with acetazolamide (PDB entry 1azm) were downloaded from the Brookhaven Protein Data Bank. The structures of ligands **L1** and **L2** were first subjected to the energy minimization by the aid of Discover. The sulfonamide rings of **L1** and **L2** were superimposed with the enzyme-bound acetazolamide. The ribbon diagram of Figure 2 with bound ligands was created with Insight II. The surface topologies of hCA-I (PDB entry 1azm) and hCA-II (PDB entry 1IF4) in Figure 1 were created with GRASP (*17*).

RESULTS

To probe whether the attachment of iminodiacetate (IDA)-conjugated Cu^{2+} to benzenesulfonamide (via spacers) invariably enhanced the binding affinities of resultant two-prong ligands for recombinant human carbonic anhydrase I (hCA-I) (*15*), we synthesized two ligands, **L1** and **L2** (Schemes 1 and 2).

There was no preconceived bias in incorporating different types of spacers in **L1** versus **L2** ligands. The only theme in synthesizing these ligands was to maintain a different distance between the individual prongs (i.e., benzenesulfonamide and IDA$-Cu^{2+}$) of the two-prong ligands. A detailed account of syntheses of **L1** and **L2** and their analyses are given in Experimental Procedures. The structures of **L1** and **L2** were computationally soaked in five layers of water, and subjected to the energy minimization by the aid of Discover-98. The distances between the NH_2 group of benzenesulfonamide and Cu^{2+} of the energy-minimized structures of **L1** and **L2** were determined to be 29 and 22 Å, respectively. The distance was primarily due to the difference in the spacer chain lengths in the above ligands. To compare the spatial locations of **L1** and **L2** upon binding of their benzenesulfonamide groups to the active site of hCA-I, we superimposed the latter group with the enzyme-bound acetazolamide of the X-ray crystallographic structure (PDB entry 1azm) (*29*). As shown in Figure 2, the IDA$-Cu^{2+}$ groups of both the ligands protrude away from the active site of the enzyme. Because of the longer spacer chain length in **L1** versus **L2**, the IDA$-Cu^{2+}$ group of the former ligand extends farther than that of the latter.

The question of whether the difference in the spacer chain length of the above ligands made a minimal or significant contribution to the affinity for their cognate enzyme site arose. If the IDA$-Cu^{2+}$ moiety of **L1** and/or **L2** could loop around and interact with one of the surface-exposed histidine residues, their binding affinities would be higher than that of the parent compound, benzenesulfonamide. To probe this,

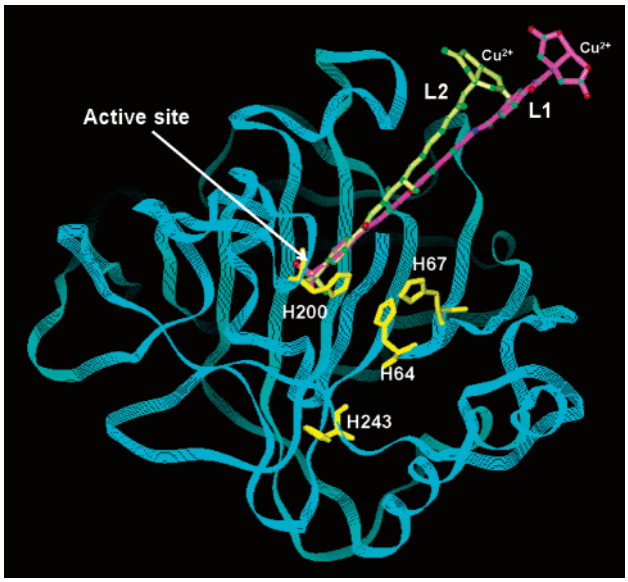

FIGURE 2: Ribbon structure of human carbonic anhydrase I with modeled two-prong ligands **L1** and **L2**. The surface-exposed histidine residues are shown. The benzenesulfonamide groups of the ligands were superimposed with the active site resident acetazolamide ring. Part of the spacers and IDA$-Cu^{2+}$ moieties of the ligands are shown to protrude away from the enzyme surface.

Scheme 2: Synthesis of Ligand **L2**

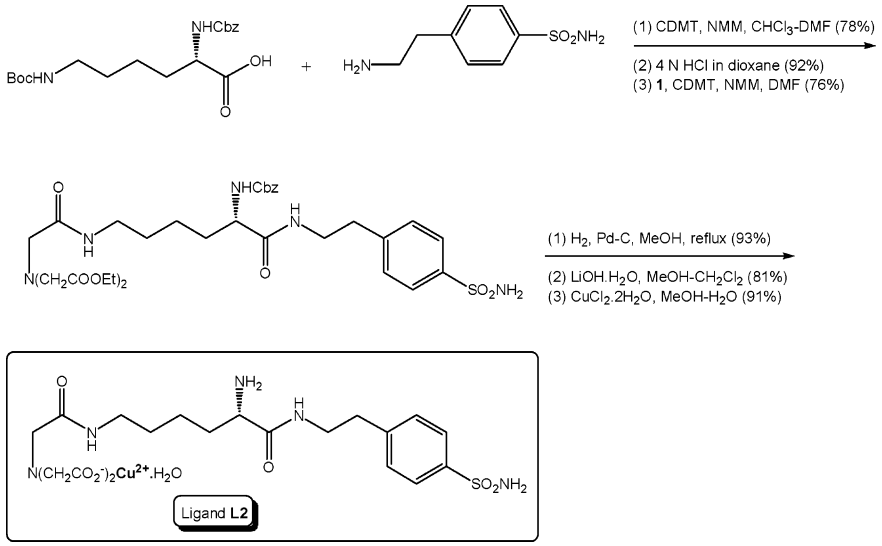

we determined the binding affinities of **L1**, **L2**, and benzenesulfonamide by performing fluorescence titration and steady-state kinetic experiments.

Enzyme−Ligand Interactions Assessed via the Fluorescence Titration Method. It has been known that the binding of dansylamide to carbonic anhydrases results in the blue shift of its fluorescence emission spectrum (λ_{ex} = 330 nm) from 536 to 468 nm, presumably due to the electronic structural changes (resulting from the deprotonation of the NH_2 group of the sulfonamide moiety) of the fluorophore within the enzyme site (*30*−*32*). Figure 3 shows the fluorescence emission spectra of 10 μM dansylamide (λ_{ex} = 330 nm) in the absence (curve 1) and presence (curve 2) of 1 μM hCA-I. Note a marked increase in the fluorescence emission intensity at 448 nm, coupled with the blue shift in the emission maximum. Although a qualitatively similar blue shift was observed in the presence of hCA-II, the fluorescence emission intensity in the latter case was ∼5-fold lower (curve 3) than that observed with hCA-I. The above difference could be either due to the difference in the level of saturation of hCA-I versus hCA-II by dansylamide under the experimental condition of Figure 3 or due to the difference in the quantum yield of the fluorophore bound to the above enzyme sites. To discriminate between these possibilities, as well as to quantitatively determine the dissociation constant of the hCA-I−dansylamide complex (the parameter essential for determining the binding affinities of different ligands), we titrated a fixed concentration of hCA-I (1 μM) with increasing concentrations of the fluorophore (Figure 3, inset). Since during this titration the concentration of the enzyme was comparable to that of dansylamide, the binding isotherm was analyzed by a complete solution of the quadratic equation, as elaborated by Qin and Srivastava (*25*). The solid smooth line is the best fit of the data for the dissociation constant (K_d) of the hCA-I−dansylamide complex being equal be 0.48 μM, and the maximum fluorescence changes (ΔF_{max}) of 80. These values are significantly different than the K_d and ΔF_{max} of 3.2 μM and 18, respectively, of the hCA-II−dansylamide complex (*15*). Clearly, under our experimental condition, dansylamide binds ∼7-fold more tightly to hCA-I than to hCA-II. In addition, since the ΔF_{max} of the hCA-I−dansylamide complex is ∼4-fold higher than that of the hCA-II−dansylamide complex, it is evident that the difference in the amplitude of the fluorescence emission of Figure 3 (in hCA-I vs hCA-II) is not due to the level of saturation of the enzyme by the fluorophore. Instead, it is due to the difference in the quantum yield of the fluorophore bound to hCA-I versus the hCA-II enzyme site.

Because of the competitive displacement of the enzyme-bound dansylamide by the benzenesulfonamide derivatives, the binding affinities of the latter could be determined by monitoring the changes in the fluorescence emission intensity at 448 nm. Figure 4 shows the titration of a mixture of hCA-I (0.25 μM) and dansylamide (10 μM) by increasing concentrations of selected ligands. Note that as the concentration of ligands increases, the fluorescence emission intensity at 448 nm (λ_{ex} = 330 nm) decreases. It is noteworthy that the decrease in the fluorescence intensity is most pronounced (at low concentrations of the ligands) with **L2**, and least pronounced with benzenesulfonamide, suggesting that **L2** can displace dansylamide from the enzyme site more easily than benzenesulfonamide. On the basis of the titration profiles of Figure 4, it is apparent that the relative strength of the binding of ligands to the enzyme is in the following order: **L2** > **L1** > benzenesulfonamide. To quantitatively determine the dissociation constants of the individual enzyme−ligand complexes, we analyzed the data of Figure 4 by eq 2. The solid smooth lines are the best fit of the data for the dissociation constants of the enzyme−benzenesulfonamide (●), enzyme−**L1** (△), and enzyme−**L2** (■) complexes being equal to 4.5 μM, 1.1 μM, and 17 nM, respectively. Given these parameters, it is apparent that whereas the dissociation constant of **L1** is only 4-fold lower than that of benzenesulfonamide, the dissociation constant of **L2** is ∼260-fold lower. Since benzenesulfonamide and IDA−Cu^{2+} moieties are common to both **L1** and **L2** ligands, the origin of the above difference must lie in the nature and/or chain length of the intervening spacer residues.

To ascertain the contribution of the IDA-chelated Cu^{2+} of **L1** and **L2** in the binding affinity, we performed the titration experiments described above in the presence of 5 mM EDTA. Due to the stronger binding affinity of EDTA (as compared to IDA) for Cu^{2+} (*33*), coupled with the mass

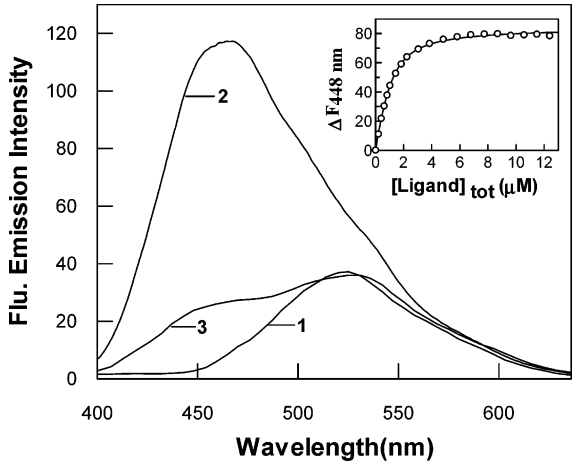

FIGURE 3: Fluorescence emission spectra of dansylamide in the absence (1) and presence of hCA-I (2) and hCA-II (3). [Dansylamide] = 10 μM. [hCA-I] = 1 μM. [hCA-II] = 1 μM. λ_{ex} = 330 nm. The inset shows the binding isotherm of the hCA-I−dansylamide complex. The increase in fluorescence emission intensity at 448 nm (λ_{ex} = 330 nm) for the titration of 1 μM hCA-I with increasing concentrations of dansylamide (total) is shown. The solid smooth line is the best fit of the experimental data (*26*) for the K_d value of 0.48 ± 0.017 μM.

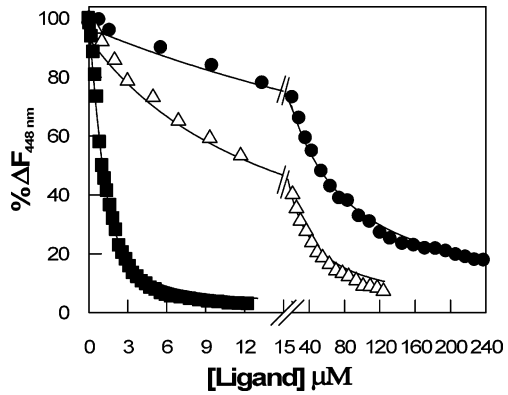

FIGURE 4: Determination of the dissociation constants of the hCA-I−ligand complexes by the dansylamide displacement method. Filled circles, empty triangles, and filled squares represent the data for benzenesulfonamide, **L1**, and **L2**, respectively. [hCA-I] = 0.25 μM. [dansylamide] = 6 μM. The K_d values of the enzyme−ligand complexes were determined by the best fit of the data (—) by eq 1. The K_d values of benzenesulfonamide, **L1**, and **L2** were determined to be 4.5 ± 0.1 μM, 1.1 ± 0.04 μM, and 17 ± 1 nM, respectively.

action effect, Cu^{2+} would be transferred from IDA to the EDTA site. EDTA does not impair the catalytic activity of the enzyme (data not shown) presumably due to the kinetic and thermodynamic stabilities of the active site resident Zn^{2+} in carbonic anhydrases (*34*). As shown in Table 1, in the presence of EDTA, the dissociation constants of **L1** and **L2** are increased from 1.1 to 4.6 μM and from 17 nM to 1.3 μM, respectively. Hence, when Cu^{2+} is stripped from the IDA moiety of the above ligands, their dissociation constants are increased. However, the above increase is more pronounced (by ~100-fold) in the case of **L2** as compared to **L1**. Obviously, Cu^{2+} of **L2** has a significantly greater energetic contribution for its binding to the enzyme than that of **L1**.

Acetazolamide has been known to be a potent inhibitor of carbonic anhydrases (particularly for hCA-II), and it has currently been used as a drug for the treatment of glaucoma (*12*). To compare the relative binding affinity of acetazolamide to that of our two-prong ligands (**L1** and **L2**), we performed the above dansylamide displacement experiment. The analysis of the data yielded the K_d value of acetazolamide (775 nM), which is similar to its K_i value reported in the literature (*35*). Hence, although the binding affinity of acetazolamide is comparable to that of **L1**, it is considerably lower than that of **L2**.

Table 1: Summary of the K_d and K_i Values of Different Ligands[a]

ligand	K_d (μM)	K_i (μM)
benzenesulfonamide	4.5 ± 0.1	3.3 ± 0.27
L1	1.1 ± 0.04	1.2 ± 0.08
L2	0.017 ± 0.001	0.027 ± 0.01
L1 and EDTA	4.6 ± 0.44	4.5 ± 0.17
L2 and EDTA	1.3 ± 0.14	1.7 ± 0.64
acetazolamide	0.78 ± 0.055	0.95 ± 0.035

[a] For the binding to human carbonic anhydrase I.

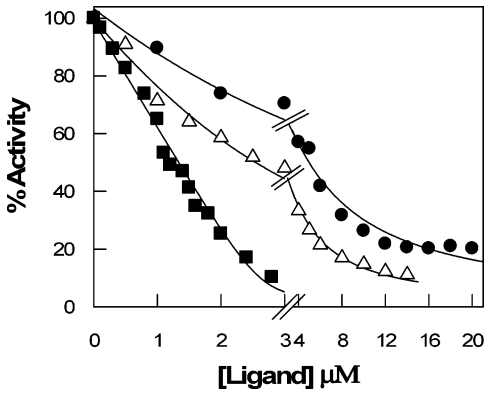

FIGURE 5: Steady-state kinetics for the inhibition of hCA-I by different ligands. The initial rates (represented as the percent activity) of the enzyme-catalyzed hydrolysis of *p*-nitrophenyl acetate were measured as a function of the ligand concentrations. [hCA-I] = 2.75 μM. [*p*-Nitrophenyl acetate] = 1 mM. The solid smooth lines are the best fit of the data according to eq 2 for the K_i values of benzenesulfonamide (●), **L1** (△), and **L2** (■) of 3.3 ± 0.27, 1.2 ± 0.08, and 0.027 ± 0.01 μM, respectively.

Steady-State Kinetic Experiments. Many carbonic anhydrases, including hCA-I, catalyze an easily detectable esterase reaction, which is monitored at 348 nm utilizing *p*-nitrophenyl acetate as a chromogenic substrate (*23*). Although the esterase reaction is not a physiological reaction of the enzyme, it is frequently utilized to measure the inhibitory potencies of different sulfonamide derivatives (*35*). To confirm that the binding affinities of different ligands, determined by the dansylamide displacement method (Figure 4 and Table 1), are reflected in their inhibitory potencies, we performed the steady-state kinetic experiments of the hCA-I-catalyzed esterolytic reaction in the presence of increasing concentrations of different ligands. Figure 5 shows the initial rates (represented as the percent of the enzyme activity) of the enzyme catalyses as a function of selected ligand concentrations. For direct comparison with the dansylamide displacement experiments, we utilized benzenesulfonamide (●), **L1** (△), and **L2** (■) as inhibitors. Since these experiments were performed at relatively high concentrations of the enzyme (because of the low turnover rate of the esterolytic reaction), the inhibition data were analyzed by eq 3. The analysis of the data yielded values of the inhibition constants (K_i) for benzenesulfonamide, **L1**, and **L2**, 3.3 μM, 1.2 μM, and 27 nM, respectively. We further performed the steady-state kinetic studies for the inhibition

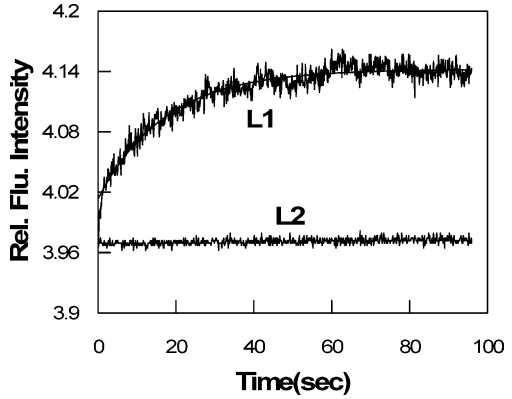

FIGURE 6: Dissociation off rates of two-prong ligands from hCA-I. The stopped-flow fluorescence traces (λ_{ex} = 330 nm, cutoff filter = 395 nm) upon mixing of the enzyme−ligand complexes with dansylamide are shown. Traces L1 and L2 represent the dissociation of **L1** and **L2** from the enzyme site, respectively. The concentrations of the enzyme and dansylamide after mixing were 0.2 and 100 μM, respectively. The concentrations of **L1** and **L2** after mixing were 2 and 1 μM, respectively. The solid smooth line of trace L1 is the best fit of the data for a rate constant of 0.058 ± 0.013 s^{-1}.

of the enzyme by azetazolamide, as well as **L1** and **L2** in the presence of 5 mM EDTA, and analyzed the data as described above. All these values along with the dissociation constants of the enzyme−ligand complexes (determined by the dansylamide displacement method) are summarized in Table 1. Note a marked similarity between the K_d and K_i values of the individual ligands, suggesting that all the ligands utilized herein competitively bind (both against dansylamide as the fluorescent probe and against *p*-nitrophenyl acetate as the substrate) to the enzyme site. The above similarity also eliminates the possibility of some unforeseen kinetic complexity arising from the interaction of one ligand or the other with the enzyme site.

Transient Kinetics for the Dissociation of the Two-Prong Ligands from the Enzyme Site. To probe whether the marked stability of **L2** (vis-à-vis **L1**) in the ground state (Figures 4 and 5) is also reflected in their dissociability from the enzyme site, we performed the stopped-flow transient kinetic experiments for measuring their dissociation off rates. These experiments were performed by mixing the individual enzyme−ligand complexes with high and excessive concentrations of dansylamide. Under this situation, the mass action would drive the overall equilibrium to the E−dansylamide complex, and the rate of formation of the latter species would serve as the measure of the dissociation off rate (k_{off}) of the corresponding enzyme−ligand complex (eq 4).

$$\text{E-L} \xrightleftharpoons{k_{off}} \text{E} + \text{L} \quad + \quad \text{Dansylamide} \quad \downarrow \quad \text{E-Dansylamide} \tag{4}$$

Since the binding of dansylamide to the enzyme yields the fluorescence emission signal at 448 nm (see Figure 3), the time course of the competitive displacement of the enzyme-bound ligands (by dansylamide) could be easily determined. Figure 6 (trace **L1**) shows the stopped-flow trace for the mixing of the enzyme−**L1** complex ([E] = 0.1 μM, [**L1**] = 2 μM) with dansylamide (100 μM). The solid smooth line is the best fit of the experimental data according to the single-exponential rate law, with a rate constant of 0.058 s^{-1}. When we performed the above experiment involving **L2** ([E] = 0.1 μM and [**L2**] = 1 μM vs [dansylamide] = 100 μM), we could not detect any increase in the fluorescence signal for ∼100 s (Figure 6, trace L2). Although, for technical reasons, we could not accurately determine the dissociation off rate of **L2** from the enzyme site, it is obviously much slower than that of **L1**. It is known that the binding of different sulfonamide derivatives (including dansylamide) to the active site of the enzyme involves changes in their electronic structures (*34*). We recently demonstrated that such electronic structural changes proceed via two steps: formation of the enzyme−ligand encounter/Michaelis complex followed by a slow isomerization step (our unpublished results). Upon consideration that the slow dissociation of ligands (with concomitant changes in their electronic structures) involves activation energy barriers, it is apparent that besides significantly stabilizing the ground state, **L2** also stabilizes the putative transition state of the enzyme−ligand complex.

Isothermal Titration Microcalorimetric Studies. Given that the IDA−Cu^{2+} moiety of **L2** significantly stabilizes both the ground and transition states of the enzyme−ligand complexes, it was of interest to determine whether the free energy changes of the above enzyme−ligand interaction were dominated by enthalpic or entropic contributions. To ascertain this, we performed the isothermal titration microcalorimetric studies for the binding of **L2** to hCA-I. In a preliminary manner, we established that the binding of both benzenesulfonamide and the IDA−Cu^{2+} moiety to hCA-I produced heat signals (exothermic peaks). Since **L2** contains benzenesulfonamide and IDA−Cu^{2+} moieties, the overall heat signal was expected to be contributed by the binding of both these moieties to their respective sites on hCA-I. Figure 7 shows the isothermal microcalorimetric titration of 11 μM hCA-I by 30 aliquots (4 μL each, except for the first aliquot which was 1 μL) of **L2** (stock concentration of 359 μM). The top panel shows the raw calorimetric data, denoting the amount of heat produced (negative exothermic peaks) following each injection of **L2** to the enzyme solution. The area under each peak represents the amount of heat produced upon binding of **L2** to the enzyme. Note that as the titration progresses, the area under the peaks becomes smaller due to the formation of the hCA-I−**L2** complex. The bottom panel of Figure 7 shows the plot of the amount of heat generated per injection as a function of the molar ratio of **L2** to hCA-I. A casual inspection of the titration data revealed that the overall binding isotherm is constituted of at least two phases. This was not surprising since **L2** contained at least two interacting regions, namely, benzenesulfonamide and the IDA−Cu^{2+} moiety, for binding with the enzyme. This feature was further apparent in our inability to fit the ITC binding data by the one-site binding model. However, the data could be reliably fitted (solid smooth line) according to the two-binding site model (*27*), yielding N_1, N_2, K_{a1}, K_{a2}, $\Delta H°_1$, and $\Delta H°_2$ values of 0.53, 2.2, 5.2 × 10^7 M^{-1}, 4.7 × 10^5 M^{-1}, −14.5 kcal/mol, and −5.6 kcal/mol, respectively. Of these parameters, the magnitudes of N_1, K_{a1}, and $\Delta H°_1$ were assigned to the binding of **L2** via both prongs. The K_d

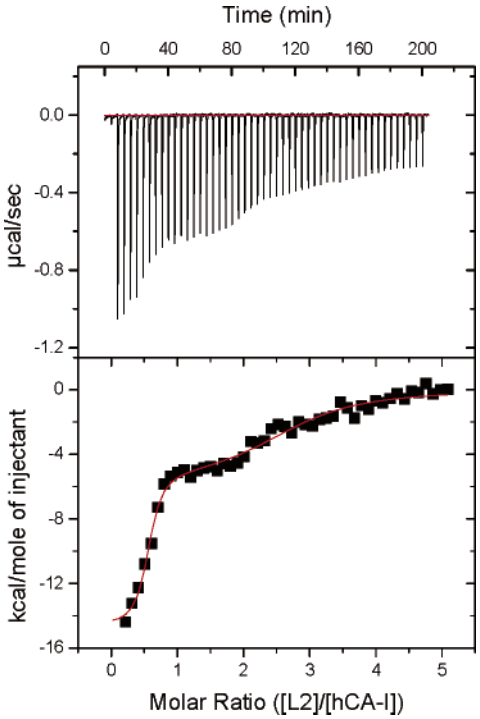

FIGURE 7: Isothermal titration microcalorimetric studies for the binding of **L2** to hCA-I. The top panel shows the raw data, generated by titration of 1.8 mL of 11 μM hCA-I by 30 injections (first injection, 1 μL; subsequent injections, 4 μL each) of 359 μM **L2**. The area under each peak was integrated and plotted against the molar ratio **L2** to hCA-I in the bottom panel. The solid smooth line is the best fit of the data according to the two-binding site model for the following stoichiometries (N_1 and N_2), association constants (K_{a1} and K_{a2}), and enthalpic changes ($\Delta H°_1$ and $\Delta H°_2$). The values of N_1, N_2, K_{a1}, K_{a2}, $\Delta H°_1$, and $\Delta H°_2$ were determined to be 0.53 $\pm$ 0.018, 2.2 $\pm$ 0.094, (5.2 $\pm$ 1.9) $\times$ 10^7 M^{-1}, (4.7 $\pm$ 1.3) $\times$ 10^5 M^{-1}, -14.5 ± 0.54 kcal/mol, and -5.6 ± 0.42 kcal/mol, respectively. When the ITC data were analyzed by adjusting the enzyme concentration to 6.1 μM (to account for the 45% inactivation of the enzyme during the 1 h time course of the ITC titration experiment), the values of N_1, N_2, K_{a1}, K_{a2}, $\Delta H°_1$, and $\Delta H°_2$ were 0.9 $\pm$ 0.03, 4.1 $\pm$ 0.5, (3.0 $\pm$ 0.6) $\times$ 10^7 M^{-1}, (4.5 $\pm$ 1.8) $\times$ 10^5 M^{-1}, -16.2 ± 0.73 kcal/mol, and -5.6 ± 0.52 kcal/mol, respectively.

($1/K_{a1}$ = 19.3 nM) value derived from these data is similar to the K_d and K_i values of 17 and 27 nM, respectively, determined from fluorescence titration (Figure 4) and steady-state kinetic experiments (Figure 5). However, of above parameters, the stoichiometry (N_1) of the first phase appeared to be ~50% of that expected for the binding of 1 mol of **L2** per mole of hCA-I. To ascertain whether the lower stoichiometry of the hCA-I−**L2** complex was due to the inactivation of hCA-I (due to the prolonged microcalorimetric titration experiment), we determined the activity of the enzyme as a function of time (data not shown). The time-dependent activity profile revealed that ~45% of the enzyme activity was indeed lost during the 1 h time regime (the time required for the completion of the first phase; see Figure 7, top panel) of our microcalorimetric titration. Given this information, when we reanalyzed the data of Figure 7 (by adjusting the concentration of the enzyme), we determined the stoichiometry of the first phase of the hCA-I−**L2** complex to be 0.90, and the K_{a1} and $\Delta H°_1$ values as being 3.0 $\times$ 10^7 M^{-1} and −16.2 kcal/mol, respectively. Although the latter values are somewhat different from those obtained previously (i.e., without adjusting the enzyme concentration to reflect the loss of the enzyme activity during microcalorimetric titration), the experimental outcomes from both data sets essentially yield the same (qualitative) conclusion, i.e., that the overall binding of **L2** to hCA-I is dominated by enthalpic rather than entropic changes (see the Discussion).

Diethyl Pyrocarbonate Treatment of the Enzyme. On the basis of a variety of circumstantial evidence (*36*−*39*), our working hypothesis has been that the IDA−Cu^{2+} moiety of the two-prong ligands binds to one of the surface-exposed histidine residues of carbonic anhydrases (*14*−*16*), resulting in the enhanced binding affinity of the active site-directed ligands (e.g., benzenesulfonamide). However, so far, we did not have experimental evidence to justify the fact that the IDA−Cu^{2+} moiety of ligands indeed interacts with one of the surface-exposed histidine residues of the enzymes (e.g., hCA-I or hCA-II) (*14*−*16*). To probe the above feature, we performed the binding studies of **L2** after treating hCA-I with diethyl pyrocarbonate (DEPC). The DEPC treatment of hCA-I was expected to modify all the surface-exposed histidine residues of the enzyme. If any such histidine residues were involved in the enhanced binding of **L2**, the above treatment would impair the enhanced binding effect contributed by the IDA−Cu^{2+} group of the ligand. Figure 8 shows the dansylamide displacement experiment for the binding of **L2** (■) to the DEPC-treated enzyme. The analysis of the data by eq 2 (smooth line) yielded a value of 1.38 μM for the dissociation constant of the enzyme−ligand complex. Note that the latter value is in marked contrast to the dissociation constant of the native enzyme−**L2** complex (17 nM). Clearly, the DEPC treatment of the enzyme decreased the binding affinity of **L2** by ~80-fold. As a hindsight control, we performed a similar experiment for the binding of benzenesulfonamide (●) to hCA-I, and discerned its dissociation constant to be 5.25 μM. Clearly, the DEPC modification of the enzyme did not impair its ability to bind benzenesulfonamide. This coupled with the fact (see Table 1) that the enhanced affinity of **L2** for hCA-I is mediated via the IDA-conjugated Cu^{2+}, it is clear that the IDA−Cu^{2+} moiety of **L2** interacts with one of the surface-exposed histidine residues of hCA-I.

To further determine how many histidine residues (*52*−*54*) are protected upon binding of **L2** to hCA-I, we titrated a fixed concentration of the enzyme (10 μM) with increasing concentrations of DEPC, and monitored the increase in absorption at 242 nm as a function of time until it reached a constant value (*54*). A control experiment was performed in which DEPC was incubated with buffer (without the enzyme). The difference in absorption (at 242 nm) between the sample and control was plotted as a function of the ratio of DEPC to hCA-1 (Figure 9). Since the two-prong inhibitor binds at both the active site (harboring three histidine residues) and the peripheral site, the DEPC modification was performed in the presence of saturating concentrations of either benzenesulfonamide (Figure 9, trace 1) or **L2** (Figure 9, trace 2). In this way, the active site histidine residues were subjected to an identical protection (against DEPC modification) by benzenesulfonamide. The data of Figure 9 show that in both cases, ΔA_{242} initially increases linearly as a function of the ratio of DEPC to hCA-I, and then it attains a plateau due to modification of all histidine residues. The intersection points of these plots correspond to the 8.2 and 6.8 modifications of histidine residues in the presence of benzenesulfon-

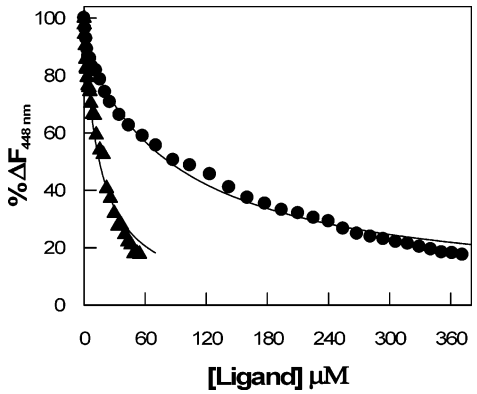

FIGURE 8: Determination of the dissociation constants of the diethyl pyrocarbonate-modified hCA-I−ligand complexes by the dansylamide displacement method. Filled circles and filled triangles represent the data of benzenesulfonamide and **L2**, respectively. [DEPC-treated hCA-I] = 0.5 μM. [Dansylamide] = 6 μM. The K_d values of the enzyme−ligand complexes were determined by the best fit of the data according to eq 2. These values for benzenesulfonamide and **L2** were found to be 5.25 ± 0.16 and 1.38 ± 0.054 μM, respectively.

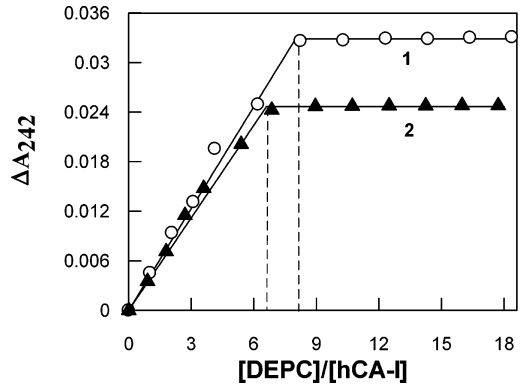

FIGURE 9: Covalent modification of histidine residues of hCA-I by diethyl pyrocarbonate (DEPC). The enzyme (10 μM) was titrated with increasing concentrations of DEPC in 0.1 M sodium phosphate buffer (pH 6.0), and the increase in absorption at 242 nm was noted as a function of time. The control experiment was performed by incubating an equal concentration of DEPC in the buffer. The difference in absorption between the sample and buffer at 242 nm was plotted as a function of the ratio of DEPC to hCA-1. The data of plots 1 (○) and 2 (▲) represent the experiments performed in the presence of 50 μM benzenesulfonamide and 20 μM **L2**, respectively. The solid lines are the linear regression analyses of the data. The intersection points represent the modification of 8.2 and 6.8 mol of histidine residues per mole of hCA-I in the presence of benzenesulfonamide and **L2**, respectively.

amide (trace 1) and **L2** (trace 2), respectively. Evidently, **L2** protects 1.4 more histidine residues than benzenesulfonamide. These data support the notion that the IDA−Cu^{2+} moiety of **L2** interacts with "one" surface-exposed histidine residue of hCA-I. We are currently performing the site specific mutations of different histidine residues of hCA-I to probe which histidine residue is specifically involved in the above interaction, and we will report this finding subsequently.

DISCUSSION

The experimental data presented herein are the first detailed studies for the binding of two-prong ligands to human carbonic anhydrase I (hCA-1), unraveling the roles of the spacer chain length and the IDA−Cu^{2+} moiety in enhancing the binding affinity of the parent ligand, benzenesulfonamide. Because of the presence of the appropriate chain length of the spacer in **L2**, and lack thereof in **L1**, the former ligand emerges as one of the most potent inhibitors of hCA-I (*1*, *35*).

Our overall experimental outcomes presented in the previous section lead to the following conclusions. (i) In two-prong ligands (**L1** and **L2**), whereas the benzenesulfonamide group binds to the active site of hCA-I, the IDA−Cu^{2+} group binds at one of the surface-exposed histidine residues. (ii) Because of the shorter spacer chain length in **L2**, the IDA−Cu^{2+} moiety finds a suitable surface-exposed histidine residue with which to interact, resulting in an ∼2 order of magnitude enhancement in the binding affinity of the parent compound, benzenesulfonamide. Such an advantage is absent with longer spacer chain-containing ligand **L1**. (iii) Besides stabilizing the ground state, the IDA−Cu^{2+} group of **L2** also stabilizes the putative transition state of the enzyme−ligand complex, which is evident by the marked disparity between the dissociation off rate constants of the enzyme−**L1** versus enzyme−**L2** complexes. (iv) Either the chelation of Cu^{2+} (of **L2)** by EDTA or the treatment of the enzyme with diethyl pyrocarbonate increases the dissociation constant of the hCA-I−**L2** complex to the level of that of benzenesulfonamide. (v) Although a major fraction of the overall energetic contribution in the binding of **L2** to hCA-I comes from the interaction of the IDA-conjugated Cu^{2+} to the histidine residues, there is a small (albeit finite) energetic contribution of the aliphatic spacer chain length of the ligand. The energetic contribution of the spacer is also apparent in the case of **L1**, although the IDA−Cu^{2+} group of the latter ligand fails to interact with any surface-exposed histidine residue. (vi) Isothermal titration microcalorimetric data reveal that there are at least two classes of binding sites of **L2**, of which the tightest binding site with maximum enthalpic changes is given by the binding of the ligand via both prongs. (vii) The overall free energy changes for the binding of **L2** to hCA-I are dominated by enthalpic rather than entropic contributions.

It has been known that at neutral pH (and in aqueous environment), the imidazole groups of histidines interact strongly with the transition metal cations (*38*, *39*). At higher pH values, other basic groups of amino acid side chains (or N-terminal group) exhibit the potentials to interact with the transition metal ions, as well as their IDA-chelated adducts. Since the imidazole group of histidine has a pK_a of 6.8, it serves as an ideal ligand for interaction with the IDA−Cu^{2+} moiety at neutral pH. By using the diethyl pyrocarbonate-modified proteins, Arnold and her collaborators have shown (via the ESR spectroscopy) that the native proteins are targeted to IDA−Cu^{2+} lipid assemblies through coordination by surface histidines (*37*, *38*). Recently, by employing ^{1}H and ^{15}N NMR techniques, Nomura et al. (*39*) have explicitly demonstrated that, at neutral pH, the IDA−Cu^{2+} moiety selectively interacts with His-68 on the surface of ubiquitin. These data are in accord with our demonstration (Figure 8) that diethyl pyrocarbonate-treated hCA-I does not bind **L2** as tightly as the native enzyme. In fact, the binding affinity of **L2** being similar to that of benzenesulfonamide suggests that there is hardly any contribution of the spacer residue as well as the IDA−Cu^{2+} moiety when hCA-I is modified by diethyl pyrocarbonate. These results corroborate our working hypothesis that the enhanced binding of the two-prong ligand

(e.g., **L2**) is primarily due to the interaction of the IDA−Cu^{2+} moiety with one of the surface-exposed histidine residues of the enzyme.

Of 11 histidine residues present in the primary structure of hCA-I, three (His-94, His-96, and His-119) are involved in stabilizing the active site Zn^{2+}, four (His-64, His-67, His-200, and His-243) are present in the vicinity of the active site pocket (which are shown in Figure 1), and the remaining four (His-40, His-103, His-107, and His-122) are confined on the opposite side of the active site pocket. Since the DEPC treatment of the enzyme in the presence of benzenesulfonamide and **L2** modifies only 8.2 and 6.8 histidine residues, respectively (see Figure 9), it appears that the three active site resident histidine residues remain unmodified. This is not surprising since these histidine residues interact tightly with the active site Zn^{2+}, and they may be further protected upon binding of benzenesulfonamide at the active site pocket. Since **L2** contains both benzenesulfonamide and IDA−Cu^{2+} moieties, its influence in further reduction of the DEPC modifiable histidine residue (from 8.2 to 6.8) is likely to be due to a strong interaction the IDA−Cu^{2+} prong of **L2** with one surface-exposed histidine residue of the enzyme.

In general, sulfonamide derivatives are weak inhibitors of hCA-I vis-à-vis hCA-II. For example, whereas the inhibition constant of one of the anti-glaucoma drugs, acetazolamide, for hCA-I is around 900 nM (950 nM as determined during our studies), that for hCA-II is ~12 nM (*40*). Scozzafava et al. (*40*) has compiled a list of more than 200 inhibitors of carbonic anhydrase isozymes with dissociation constants in the nanomolar range. In comparison, it is clearly apparent that our two-prong ligand, **L2,** certainly falls in the category of one of the most potent inhibitors of hCA-I (K_d = 17 nM, K_i = 27 nM).

One of the most intriguing aspects of our investigation is the differential binding affinity of **L1** versus **L2** for hCA-I. Whereas the attachment of the IDA−Cu^{2+} moiety to benzenesulfonamide via one type of spacer (as in **L1**) does not markedly affect its binding affinity for hCA-I, the use of the other type of spacer (as in **L2**) increases its binding affinity by ~2 orders of magnitude. A casual comparison of the structures of these ligands reveals that they differ both by the chain length of the spacers and by their chemical compositions. In principle, both these factors have potentials to contribute to the binding affinities of the enzyme−ligand complexes. If a spacer group is not of the appropriate chain length, the IDA−Cu^{2+} moiety of the two-prong ligand would not be able to find its complementary anchor site (i.e., histidine residue) on the surface of the enzyme. However, because of the intrinsic flexibility of the spacer groups, there is always a possibility of the adjustment in the ligand structure such that the IDA−Cu^{2+} moiety finds its interacting (histidine) partner. Such a possibility would also be dependent on the spatial distribution of the surface-exposed histidine residues. If the histidine residues are closely spaced on the protein surface (as in hCA-II; see Figure 1), the spacer based selectivity in the two-prong ligands would not be as pronounced as in the proteins containing scattered histidine residues (such as in hCA-I; see Figure 1). This has been the dominant feature in selecting hCA-I in preference to hCA-II in this investigation.

Besides, depending upon the spatial location, the difference in the chemical nature of the spacers can have different types

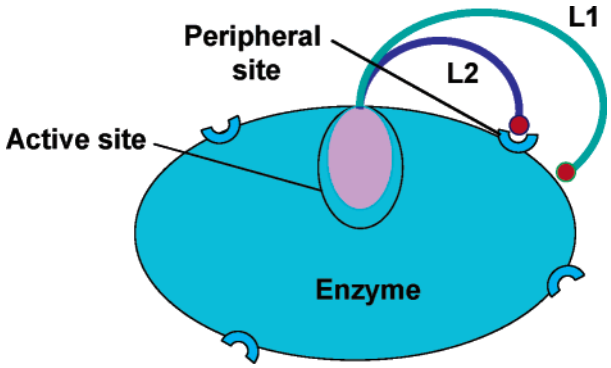

FIGURE 10: Cartoon of the spacer-based selectivity for the binding of two-prong ligands to hCA-I. These ligands bind at both active and peripheral sites of the enzyme. Whereas the second prong of the shorter spacer chain-containing ligand could easily loop around and interact at a complementary peripheral site, that of the longer spacer-containing ligand fails to find complementary interacting site on the surface of the enzyme.

of binding interactions at the protein surface. However, since the Cu^{2+} free **L1** (generated in the presence of EDTA) exhibits a binding affinity for hCA-I similar to that of benzenesulfonamide, it appears that the chemical nature of the spacer (containing triethylene glycol, an amide linkage, and an aromatic group) in **L1** has practically no independent energetic contribution to the overall binding affinity. On the contrary, the Cu^{2+} free **L2** still shows 3−4-fold higher binding affinity than benzenesulfonamide, suggesting a small (albeit finite) energetic contribution of the aliphatic chain and/or primary amine group of the spacer to the overall binding constant. Given these, it is clear that the marked difference in the binding affinity of **L1** versus **L2** for hCA-I comes from the difference in the chain length of the spacers rather than from their chemical structures. This is schematized by the cartoon in Figure 10. As shown in this cartoon, the shorter spacer chain length-containing ligand (viz., **L2**) allows its IDA−Cu^{2+} moiety to easily loop around and find its complementary anchor site on the surface of the protein. On the other hand, due to longer chain length of spacer in **L1**, the IDA−Cu^{2+} moiety fails to loop around and find the same or another suitable anchor site on the enzyme surface, obviating the above-noted energetic advantage.

We recently performed the isothermal titration microcalorimetric studies for the binding of benzenesulfonamide as well as of the IDA−Cu^{2+} moiety to hCA-I, and observed that the individual binding isotherm conformed to one class of binding site (data not shown). Since the binding of both benzenesulfonamide and the IDA−Cu^{2+} moiety (independently) to hCA-I produces heat signals, the ITC binding isotherm for the interaction of **L2** with hCA-I was expected to be comprised of at least three different types of complexes: (i) only the benzenesulfonamide group of **L2** interacting at the active site of hCA-I and the IDA−Cu^{2+} group protruding away from the enzyme surface, (ii) only the IDA−Cu^{2+} group of **L2** interacting with different histidine residues of hCA-I and the benzenesulfonamide group protruding away from the enzyme surface, and (iii) both benzenesulfonamide and the IDA−Cu^{2+} moiety of **L2** simultaneously interacting at the active and peripheral (histidine) site of hCA-I, respectively. Of these, the latter interaction (exhibiting a dissociation constant of 17−27 nM during fluorescence titration and steady-state kinetic experi-

ments) is represented by the high-affinity binding site ($K_a = 3.0-5.2 \times 10^7\ M^{-1}$) in the binding isotherm of Figure 7. Since the ITC data could be reliably fitted by two classes of binding sites, we surmise that the second (weaker) binding site of Figure 7 contains the contribution from scenarios (i) and (ii). However, the latter interactions do not appear to reduce the stoichiometry of the DEPC-modified histidine residues per mole of hCA-I (Figure 9).

It should be noted that although hCA-I is fairly stable in the presence of different inhibitors on a short-term basis (adequate for performing most of the experiments reported herein), it tends to undergo slow inactivation in the presence of **L2**. Our preliminary data suggest that ~45% of the enzyme activity is lost during the 1 h time regime of the ITC titration experiment (Figure 7). When the latter feature is taken into account in analyzing the ITC titration data, the stoichiometry of the first phase is increased from 0.53 to 0.9, with small changes in the K_{a1} and ΔH°_1 values (see the legend of Figure 7). Assuming the standard state of 1 M, the ΔG°_1 value for the binding of **L2** to hCA-I can be calculated as being equal to −10.2 kcal/mol. Given a ΔH°_1 value of −16.2 kcal/mol, the entropic contributions ($T\Delta S^\circ$) can be calculated to be −6.0 kcal/mol. On the basis of these parameters, it is apparent that the overall binding of **L2** to hCA-I is enthalpically rather than entropically driven. It should be emphasized that this qualitative conclusion remains unaffected whether we take into account the slow inactivation of the enzyme by **L2** during the course of the ITC experiment. From a quantitative point of view, if the inactivation of the enzyme by **L2** is not taken into account in determining the ΔG°_1 and ΔH°_1 values, the latter are −10.5 and −14.5 kcal/mol, respectively, yielding a smaller (by 2 kcal/mol) entropic disadvantage. However, irrespective of the absolute magnitude of the entropic factor, we believe it is contributed by the restriction of the translational, rotational, and conformational freedoms of **L2** upon binding to the enzyme site. Hence, if the entropic loss of **L2** could be minimized (by introducing constraint in the molecule), the ΔG° would become more favorable. We are currently exploring such a possibility by introducing a few amide linkages in the spacer region to test the hypothesis described above, and we will report such findings subsequently.

Our approach of designing the two-prong ligands will find a variety of applications in pharmaceutical, agricultural, and biotechnological industries. Such applications may range from the de novo designing of highly potent and isozyme specific inhibitors as potential drugs and insecticide and herbicide agents, designing compounds which would promote and/or preclude protein−protein, protein−lipid, protein−carbohydrate, and protein−nucleic acid interactions, crystallization of membrane-bound proteins, etc. There has been some literature evidence of designing a similar type of ligand, which binds at two different regions of enzyme molecules (*48*−*51*). Interestingly, in the case of carbonic anhydrase, Jain et al. (*49*) tried to attach oligoglycine moieties with different chain lengths at the para position of benzenesulfonamide with the hope of increasing the binding affinity of the parent compound (benzenesulfonamide), but such an attempt failed, since the oligoglycine moiety of the above conjugate could not find a complementary interacting surface on the carbonic anhydrase structure (*47*). This is not surprising since the binding affinity of EDTA-treated **L2** (see Table-1) is similar to that of benzenesulfonamide, suggesting that the Cu^{2+} free tether group has practically no energetic contribution for the binding to the enzyme.

It should be emphasized that there is an intrinsic limitation in the structure-based drug design, primarily due to the inherent flexibility in the protein structure, as well as the limited geometry of the ligand binding pockets (active sites in the case of enzymes) to accommodate extensive variations in the inhibitor structures (*41*−*44*). Besides, on the basis of the structural coordinates of the selected enzyme−ligand complexes, it is difficult to predict, a priori, whether the desired changes in the inhibitor structure would be better accommodated within the active site pockets (*44*−*47*). Such limitations can be easily overcome, at least in principle, by designing the enzyme inhibitors, which would not only bind to their active site pockets but also bind (by looping around) to the surface-exposed amino acid residues. The fact that the attachment of the second prong does not invariably enhance (e.g., as in **L1** vs **L2**) the binding affinity of the parent ligand implies that the two-prong ligands can be highly selective. As is evident from these studies, the ligand-based selectivity can be incorporated by controlling the distance between the individual prongs of the ligands by selected spacer chain lengths. Hence, our overall approach can be easily extended toward developing the isozyme specific two-prong inhibitors as potential drugs, herbicides, insecticides, or other protein modulators.

REFERENCES

1. Supuran, C. T., Scozzafava, A., and Conway, J. (2004) *Carbonic anhydrase: Its Inhibitors and Activators*, CRC Press, Boca Raton, FL.
2. Supuran, C. T., Scozzafava, A., and Casini, A. (2003) Carbonic anhydrase inhibitors, *Med. Res. Rev. 23*, 146−189.
3. Chegwidden, W. R., and Carter, N. D. (2000) *The carbonic anhydrases: New Horizons*, Birkhauser Verlag, Basel, Switzerland.
4. Nishimoiri, I. (2004) *Acatalytic CAs: Carbonic anhydrase related proteins*, in *Carbonic anhydrase: Its Inhibitors and Activators* (Supuran, C. T., Scozzafava, A., and Conway, J., Eds.) pp 24−43, CRC Press, Boca Raton, FL.
5. Potter, C. P. S., and Harris, A. L. (2003) Diagnostic, prognostic and therapeutic implications of carbonic anhydrases in cancer, *Br. J. Cancer 89*, 2−7.
6. Schuman, J. (2002) Short and long-term safety of glaucoma drugs, *Expert Opin. Drug Saf. 1*, 181−194.
7. Gray, W. D., and Rauh, C. E. (1967) The anticonvulsant action of inhibitors of carbonic anhydrase: Site and mode of action in rats and mice, *J. Pharmacol. Exp. Ther. 156*, 383−396.
8. Scozzafava, A., Mastrolorenzo, A., and Supuran, C. T. (2004) Modulation of carbonic anhydrase activity and its applications in therapy. *Expert Opin. Ther. Patents 14*, 667−702.
9. Barnish, I. T., Cross, P. E., Dickinson, R. P., Gadsby, B., Parry, M. J., Randall, M. J., and Sinclair, I. W. (1980) Cerebrovasodilatation through selective inhibition of the enzyme carbonic anhydrase.2.Imidazo[2,1-b]thiadiazole and imidazo[2,1-b]thiazolesulfonamides, *J. Med. Chem. 23*, 117−121.
10. Peters, G., and Roch-Ramel, F. (1969) Thaiziide diuretics and related drugs, in *Handbook of Experimental Pharmacology*, Vol. 24, pp 257−385, Springer, Berlin.
11. Pastorekova, S., Parkkila, S., Pastorek, J., and Supuran, C. T. (2004) Carbonic anhydrases: Current State of the Art, Therapeutic Applications and Future Prospects, *J. Enzyme Inhib. Med. Chem. 19*, 199−229.
12. Herklel, U., and Pfeiffer, N. (2001) Update on topical carbonic anhydrase inhibitors, *Curr. Opin. Ophthalmol. 12*, 88−93.
13. Stams, T., and Christianson, D. W. (2000) X-ray crystallographic studiesmammalian carbonic anhydrase isozymes, in *The Carbonic Anhydrases: New Horizons* (Chegwidden, W. R., Carter, N. D.,

and Edwards, Y., Eds.) Vol. 90, pp 159−174, Birkhauser-Verlag, Basel, Switzerland.
14. Roy, B. C., Hegge, R., Rosendahl, T., Jia, X., Lareau, R., Mallik, S., and Srivastava, D. K. (2003) Conjugation of poor inhibitors with surface binding groups: A strategy to improve inhibition, *J. Chem. Soc., Chem. Commun. 18*, 2328−2329.
15. Banerjee, A. L., Swanson, M., Roy, B. C., Jia, X., Haldar, M., Mallik, S., and Srivastava, D. K. (2004) Protein surface-assisted enhancement in the binding affinity of an inhibitor for recombinant human carbonic anhydrase-II, *J. Am. Chem. Soc. 126*, 10875−10883.
16. Roy, B. C., Banerjee, A. L., Swanson, M., Jia, X. G., Haldar, M. K., Mallik, S., and Srivastava, D. K. (2004) Two-Prong Inhibitors for Human Carbonic Anhydrase, *J. Am. Chem. Soc. 126*, 13206−13207.
17. Nicholls, A., Sharp, K., and Honig, B. (1991) Protein folding and association: Insights from the interfacial and thermodynamic properties of hydrocarbons, *Proteins: Struct., Funct., Genet. 11*, 281−296.
18. Forsman, C., Behraven, G., Jonsson, B. H., Liang, Z., Lingskog, S., Ren, X., Sandstrom, J., and Wallgreen, K. (1988) Histidine 64 is not required for high CO_2 hydration activity of human carbonic anhydrase II, *FEBS Lett. 229*, 360−362.
19. Tu, C., and Silverman, D. N. (1989) Role of histidine 64 in the catalytic mechanism of human carbonic anhydrase II studied with a site specific mutant, *Biochemistry 28*, 7913−7918.
20. Engstrand, C., Jonsson, B. H., and Lindskog, S. (1995) Catalytic and inhibitor-binding properties of some active-site mutants of human carbonic anhydrase-I, *Eur. J. Biochem. 229*, 696−702.
21. Sambrook, J., Fritsch, E. F., and Maniatis, T. (2000) *Molecular Cloning: A Laboratory Manual*, Cold Spring Harbor Laboratory Press, Plainview, NY.
22. Banerjee, A. L., Swanson, M., Mallik, S., and Srivastava, D. K. (2004) Purification of recombinant human carbonic anhydrase-II by metal affinity chromatography without incorporating Histidine tags, *Protein Expression Purif. 37*, 450−454.
23. Pocker, Y., and Stone, J. T. (1967) Catalytic versatility of erythrocyte carbonic anhydrase III. Kinetic studies of the enzyme-catalyzed hydrolysis of *p*-nitrophenyl acetate, *Biochemistry 6*, 668−678.
24. Bradford, M. M. (1976) A rapid and sensitive method for the quantitation of microgram quantities of protein utilizing the principle of protein-dye binding, *Anal. Biochem. 72*, 248−254.
25. Qin, L., and Srivastava, D. K. (1998) Energetics of two-step binding of a chromophoric reaction product, *trans*-3-indoleacryloyl-CoA, to medium-chain acyl-coenzyme-A dehydrogenase, *Biochemistry 37*, 3499−3508.
26. Kumar, N. R., and Srivastava, D. K. (1995) Facile and restricted pathways for the dissociation of octenoyl-CoA from the medium-chain fatty acyl-CoA dehydrogenase(MCAD)-$FADH_2$-octenoyl-CoA charge-transfer complex: Energetics and mechanism of suppression of the enzyme's oxidase activity, *Biochemistry 34*, 9434−9443.
27. Wiseman, T., Williston, S., Brandts, J. F., and Lin, L. N. (1989) Rapid measurement of binding constants and heats of binding using a new titration calorimeter, *Anal. Biochem. 179*, 131−137.
28. Burks, E., Koshti, N., Jacobs, H., and Gopalan, A. (1998) Selective monohydrolysis of esters of polyaminocarboxylic acids using pig liver esterase, *Synth. Lett. 11*, 1285−1287.
29. Chakravarty, S., and Kannan, K. K. (1994) Drug−protein interactions. Refined structures of three sulfonamide drug complexes of human carbonic anhydrase I enzyme, *J. Mol. Biol. 243*, 298−309.
30. Chen, R. F., and Kernohan, J. C. (1967) Combination of bovine carbonic anhydrase with a fluorescent sulfonamide, *J. Biol. Chem. 242*, 5813−5823.
31. Day, Y. S. N., Baird, C. L., Rich, R. L., and Myszka, D. G. (2002) Direct comparison of binding equilibrium, thermodynamic, and rate constants determined by surface- and solution-based biophysical methods, *Protein Sci. 11*, 1017−1025.
32. Fierke, C. A., Calderone, T. L., and Krebs, J. F. (1991) Functional consequences of engineering the hydrophobic pocket of carbonic anhydrase II, *Biochemistry 30*, 11054−11063.
33. Sillen, L. G., and Martell, A. E. (1964) in *Stability Constants of Metal Ion Complexes*, 2nd ed., The Chemical Society, London.
34. Fierke, C. A., and Thompson, R. B. (2001) Fluorescence-based biosensing of zinc using carbonic anhydrase, *BioMetals 14*, 205−222.
35. Ilies, M. A., Masereel, B., Rolin, S., Scozzafava, A., Campeanu, G., Cimpeanu, V., and Supuran, C. T. (2004) Carbonic anhydrase inhibitors: Aromatic and heterocyclic sulfonamides incorporating adamantyl moieties with strong anticonvulsant activity, *Bioorg. Med. Chem. 12*, 2717−2726.
36. Frey, W., Schief, W. R., Jr., Pack, D. W., Chen, C. T., Chikotti, A., Stayton, P., Vogel, V., and Arnold, F. H. (1996) Two-dimensional protein crystallization via metal-ion coordination by naturally occurring surface histidines, *Proc. Natl. Acad. Sci. U.S.A. 93*, 4937−4941.
37. Pack, D. W., and Arnold, F. H. (1997) Langmuir monolayer characterization of metal chelating lipids for protein targeting to membranes, *Chem. Phys. Lipids 86*, 135−152.
38. Pack, D. W., Chen, G., Maloney, K. M., Chen, C. T., and Arnold, F. H. (1997) A metal-chelating lipid for 2D protein crystallization via coordination of surface histidines, *J. Am. Chem. Soc. 119*, 2479−2487.
39. Nomura, M., Kobayashi, T., Kohno, T., Fujiwara, K., Tenno, T., Shirakawa, M., Ishizaki, I., Yamamoto, K., Matsuyama, T., Mishima, M., and Kojima, C. (2004) Paramagnetic NMR study of Cu^{2+}−IDA complex localization on a protein surface and its application to elucidate long distance information, *FEBS Lett. 566*, 157−161.
40. Scozzafava, A., Menabuoni, L., Mincione, F., and Supuran, C. T. (2002) Carbonic anhydrase inhibitors. A general approach for the preparation of water-soluble sulfonamides incorporating polyamino-polycarboxylate tails and of their metal complexes possessing long-lasting, topical intraocular pressure-lowering properties, *J. Med. Chem. 45*, 1466−1476.
41. Carlson, H. A. (2002) Protein flexibility and drug design: How to hit a moving target, *Curr. Opin. Chem. Biol. 6*, 447−452.
42. Wong, C. F., and McCammon, J. A. (2003) Protein flexibility and computer-aided drug design, *Annu. Rev. Pharmacol. Toxicol. 43*, 31−45.
43. Noble, M. E., Endicott, J. A., and Johnson, L. N. (2004) Protein kinase inhibitors: Insights into drug design from structure, *Science 303*, 1800−1805.
44. Wong, C. F., and McCammon, J. A. (2003) Protein simulation and drug design, *Adv. Protein Chem. 66*, 87−121.
45. Davis, A. M., Teague, S. J., and Kleywegt, G. J. (2003) Application and limitations of X-ray crystallographic data in structure-based ligand and drug design, *Angew. Chem., Int. Ed. 42*, 2718−2736.
46. Neamati, N., and Barchi, J. J., Jr. (2002) New paradigms in drug design and discovery, *Curr. Top. Med. Chem. 2*, 211−227.
47. Sharp, K. A., Nicholls, A., Friedman, R., and Honig, B. (1991) Extracting hydrophobic free energies from experimental data: Relationship to protein folding and theoretical models, *Biochemistry 30*, 9686−9697.
48. Erlanson, D. A., and Hansen, S. K. (2004) Making drugs on proteins: Site-directed ligand discovery for fragment-based lead assembly, *Curr. Opin. Chem. Biol. 8*, 399−406.
49. Jain, A., Huang, S. G., and Whitesides, G. M. (1994) Lack of effect of the length of oligoglycine- and oligo(ethylene glycol)-derived para-substituents on the affinity of benzenesulfonamide for carbonic anhydrase II in solution, *J. Am. Chem. Soc. 116*, 5057−5062.
50. Erez, M., Takemori, A. E., and Portoghese, P. S. (1982) Narcotic antagonistic potency of bivalent ligands which contain β-Naltrexamine. Evidence for bridging between proximal recognition sites, *J. Med. Chem. 25*, 847−849.
51. Portoghese, P. S., Larson, D. L., Sayre, L. M., Yim, C. B., Ronsisvalle, G., Tam, S. W., and Takemori, A. E. (1986) Opiod agonist and antagonist bivalent ligands. The relationship between spacer length and selectivity at multiple opiod receptors, *J. Med. Chem. 29*, 1855−1861.
52. Miles, E. W. (1977) Modification of histidyl residues in proteins by diethylpyrocarbonate, *Methods Enzymol. 47*, 431−442.
53. Melchior, W. B., and Farhney, D. (1970) Ethoxyformylation of proteins. Reaction of ethoxyformic anhydride with α-chymotrypsin, pepsin, and pancreatic ribonuclease at pH 4, *Biochemistry 9*, 251−258.
54. Mazumdar, A., Bandyopadhyay, D., Badyopadhyay, U., and Banerjee, R. K. (2002) Probing the role of active site histidine residues in the catalytic activity of lacrimal gland peroxidase, *Mol. Cell. Biochem. 237*, 21−30.

BI047737B